ISSN 1674-1056
http://cpb.iphy.ac.cn
http://iopscience.iop.org/cpb
中国物理 B
Chinese Physics
中国物理
Chinese Physics B

Specific heat in superconductors

Hai-Hu Wen(闻海虎)

Citation: Chin. Phys. B . 2020, 29(1): 017401 . **doi:** 10.1088/1674-1056/ab5a3d
Journal homepage: http://cpb.iphy.ac.cn; http://iopscience.iop.org/cpb

What follows is a list of articles you may be interested in

Quantum Monte Carlo study of the dominating pairing symmetry in doped honeycomb lattice

Xingchuan Zhu(朱兴川), Tao Ying(应涛), Huaiming Guo(郭怀明), Shiping Feng(冯世平)

Chin. Phys. B . 2019, 28(7): 077401 . **doi:** 10.1088/1674-1056/28/7/077401

Fluctuating specific heat in two-band superconductors

Lei Qiao(乔雷), Cheng Chi(迟诚), Jiangfan Wang(王江帆)

Chin. Phys. B . 2017, 26(11): 117401 . **doi:** 10.1088/1674-1056/26/11/117401

Theory of specific heat of vortex liquid of high T_c superconductors

Chen Bai(白晨), Cheng Chi(迟诚), Jiangfan Wang(王江帆)

Chin. Phys. B . 2016, 25(10): 107404 . **doi:** 10.1088/1674-1056/25/10/107404

Thermodynamics around magnetic phase transitions in alternating double-chain spin systems

Ding Lin-Jie, Zhong Yuan, Fan Shuai-Wei, Zhu Li-Ya

Chin. Phys. B . 2014, 23(12): 127401 . **doi:** 10.1088/1674-1056/23/12/127401

Paraconductivity study in $ErBa_2Cu_{3-x}M_xO_{7-\delta}$ (M = Zn, Fe) superconductors

A. Sedky, S. B. Mohamed

Chin. Phys. B . 2013, 22(11): 117401 . **doi:** 10.1088/1674-1056/22/11/117401

TOPICAL REVIEW — Fundamental research under high magnetic fields

Specific heat in superconductors

Hai-Hu Wen(闻海虎)†

School of Physics, Nanjing University, Nanjing 210093, *China*

(Received 24 October 2019; accepted manuscript online 22 November 2019)

Specific heat is a powerful tool to investigate the physical properties of condensed materials. Superconducting state is achieved through the condensation of paired electrons, namely, the Cooper pairs. The condensed Cooper pairs have lower entropy compared with that of electrons in normal metal, thus specific heat is very useful in detecting the low lying quasiparticle excitations of the superconducting condensate and the pairing symmetry of the superconducting gap. In this brief overview, we will give an introduction to the specific heat investigation of the physical properties of superconductors. We show the data obtained in cuprate and iron based superconductors to reveal the pairing symmetry of the order parameter.

Keywords: specific heat, gap symmetry, low lying quasiparticle excitations, cuprates, iron based superconductors

PACS: 74.25.Bt, 74.20.Rp, 74.70.Xa, 74.72.–h **DOI:** 10.1088/1674-1056/ab5a3d

1. Introduction

Specific heat, as a bulk measurement technique, is very powerful to study the physical properties of condensed matter physics. Superconductors can be categorized into two types according to the Ginzburg–Landau parameter $\kappa = \lambda/\xi$. Superconductors with $\kappa < 1/\sqrt{2}$ belong to type-I, those with $\kappa > 1/\sqrt{2}$ belong to type-II, these associate with the positive and negative interface energies, respectively.

In type-I superconductors, the entropy which is defined as $S = -(\partial g/\partial T)_H$ is continuous at $H = 0$ and $T = T_c$, but the specific heat which is defined as $C = -T(\partial S/\partial T)_H = T\left(\partial^2 g/\partial T^2\right)_H$ has a discontinuous jump, therefore the thermodynamics transition is second order. Here g is the Gibbs free energy per volume. While in a finite magnetic field, the entropy has a discontinuous jump at $T_c(H)$, the transition is first order. Because the interface energy is positive in type-I superconductors, when the demagnetization factor is not zero, the magnetic flux will penetrate into the superconductor at the edge, and form an intermediate state with the spatially separated normal and superconducting regions.

In type-II superconductors, the interface energy between a normal state region and a superconducting region is negative, therefore the magnetic flux penetrated into the superconductor will be separated into small bundles of flux (with interface areas as much as possible), each carrying a flux quanta $\Phi_0 = h/2e = 2.07 \times 10^{-15}$ web. This state contains both the superconducting region and the normal state region. Since the superconducting region has zero or very low quasiparticle density of states (DOS), but the normal region does have DOS, therefore the specific heat can be used to detect the basic properties of the superconductors. Using specific heat under different temperature and magnetic field, one can detect the vortex melting, vortex phase transition, the low energy quasiparticle density of states, etc. Thus it is a very useful and powerful tool to investigate the basic properties of superconductors.

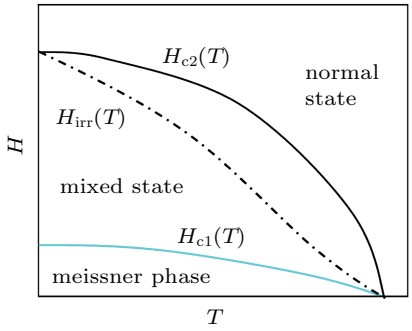


Fig. 1. The phase diagram of magnetic field versus temperature of a type-II superconductor. Here H_{c1}, H_{irr}, and H_{c2} correspond to the lower critical field, irreversibility field, and upper critical field, respectively. The area between H_{c1} and H_{c2} is called as the mixed state.

In Fig. 1, we show a typical field temperature phase diagram of a type-II superconductor. Here the H_{c1}, H_{irr}, and H_{c2} correspond to the lower critical field, irreversibility field, and upper critical field, respectively. The lower critical field is corresponding to the very first penetration of magnetic field into the superconductor. According to the Ginzburg–Landau theory, we have

$$H_{c1} = \frac{1}{4\pi\mu_0}\frac{\Phi_0}{\lambda^2}\ln\kappa. \tag{1}$$

Here λ is the London penetration depth and relates to the superfluid density as $1/\lambda^2 = m/\mu_0\rho_s e^2$. Therefore we can straightforwardly have

$$H_{c1} = \frac{\Phi_0 e^2\rho_s}{4\pi m}\ln\kappa. \tag{2}$$

†Corresponding author. E-mail: hhwen@nju.edu.cn

© 2020 Chinese Physical Society and IOP Publishing Ltd

Here the superfluid density ρ_s determines the superconducting phase stiffness or rigidity. Sometime one can use the temperature dependence of the lower critical field to detect that of the superfluid density, in order to derive the message of the superconducting gap.

The upper critical field normally has different meanings for a type-II superconductor depending on the particular situation. It generally corresponds to the formation of the droplet of Cooper pairs in a superconductor when going from high temperature and magnetic field to lower values. The Cooper pair can be broken by two different ways, one is through the orbital depairing, the other is through the spin depairing. The orbital depairing is through the Lorentz force acting on the electrons. When the Lorenz force does work on the electrons and make them depart in the distance of coherence length ξ, the Cooper pair will be broken. Thus we have

$$eH_{c2} \times 2v_F \cdot \xi = 2\Delta. \tag{3}$$

This further changes into

$$H_{c2} = \frac{\Delta}{ev_F\xi}. \tag{4}$$

Using the Pippard relation $\xi \approx \hbar v_F/\pi\Delta$, we have

$$H_{c2} = \frac{2}{\pi}\frac{\Phi_0}{2\pi\xi^2}. \tag{5}$$

One can see that, this estimate gives a value which is very close to that given by the GL theory in the high field region. In some cases, the interaction between the magnetic field and the spin of an electron may exceed the upper critical field. For a system with moderate spin–orbital coupling, this spin related pair-breaking effect may occur first. This can be estimated as

$$H_{c2}^{spin} \cdot \mu_B \approx \Delta. \tag{6}$$

Here μ_B is the Bohr magneton, the magnetic moment of an electron. Before this critical field is reached, a first order transition to normal state will occur, this field is about $H_{c2}^{spin} \times \mu_B \approx \Delta/\sqrt{2}$. Using the relation $\Delta = 1.75k_BT_c$ for the case of weak coupling BCS theory, taking $\mu_B = 9.27 \times 10^{-24}$ J/T, $k_B = 1.38 \times 10^{-23}$ J/K, we have

$$H_{c2}^{spin} \approx 1.84T_c \quad (\mathrm{T/K}). \tag{7}$$

This formula is sometime called as the Pauli limit of the upper critical field.[1,2]

In unconventional superconductors, the spin parity of the two electrons in a Cooper pair can be categorized as spin singlet or spin triplet depending on the parity of the orbital momentum. This is illustrated in Table 1.

In Table 1, 1 and 2 represent the two electrons, the upward and downward arrows represent the spin directions of the electrons. Due to the Pauli exclusive principle of the electrons, the wave-function of the two electrons in a Cooper pair should be anti-symmetric. When the spin wave function is symmetric, the momentum part should be anti-symmetric, therefore the quantum number of the orbital function will be odd, such as $l = 1, 3$ corresponding to the cases of p-wave or g-wave. However, when the spin part wave function is anti-symmetrized, the momentum part is even, corresponding to $l = 0, 2, \ldots$ Here $l = 0$ corresponds to s-wave, $l = 2$ to d-wave. The orbital wave function will take the shapes like those of the electronic orbitals in an atom. For example, for $s = 0$, it is an isotropic sphere, for a simple p_x or p_y-wave, it is a dumbbell shape with opposite signs at the two nobs, for a d-wave, it looks like two crossing dumbbells with the signs alternatively changed. In Fig. 2, we show the typical shape of the order parameter on a circular like Fermi surface surrounding the Brillouin zone center. The Cooper pairing order parameter is directly related to the pairing interaction, therefore it is fundamentally related to the pairing mechanism of superconductivity.

Table 1. The spin and momentum wave function index of a Cooper pair when the spin orbital coupling is weak.

Spin state	Description	Orbital numbers l
Spin singlet	$\uparrow(1)\downarrow(2) - \uparrow(2)\downarrow(1)$	$l = 0, 2, \ldots$
	$\uparrow(1)\uparrow(2)$	
Spin triplet	$\downarrow(1)\downarrow(2)$	$l = 1, 3, \ldots$
	$\uparrow(1)\uparrow(2) + \downarrow(1)\downarrow(2)$	

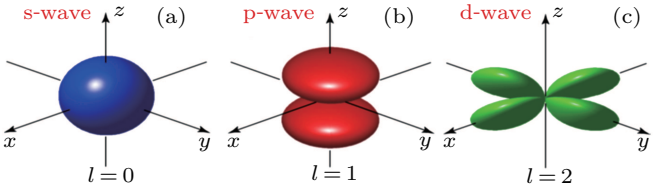


Fig. 2. The shape of orbital part of the order parameter of a Cooper pair, or pairing function with different pairing symmetries. (a) The isotropic s-wave, the gap magnitude is isotropic on everywhere of the Fermi surface. (b) The p-wave gap function with sign reversal at the two leaves. (c) The d-wave gap function with sign changing alternatively from one leaf to another.

Table 2. Gap functions of s-wave, p_z-wave, and d-wave.

Gap symmetry	l	Wave function
s-wave	0	$\Delta_s = \Delta_0$
p_z-wave	1	$\Delta_p = \Delta_0 \cos k_z$
$d_{x^2-y^2}$-wave	2	$\Delta_d = \Delta_0(\cos k_x - \cos k_y)$

By using specific heat, we can not only determine the critical fields, but also detect the symmetry of the pairing function which gives insight to the fundamental pairing mechanism.

2. Specific heat measurement techniques

2.1. Relaxation method

Specific heat can be measured by several kinds of methods, while since most of them are undertaken in vacuum, generally speaking, it is not easy. Generally, the specific heat

can be measured through adiabatic method or non-adiabatic method. Usually the adiabatic method is more challenging since the precise measurement of heat amount and temperature variation in high vacuum is quite difficult. We thus use the relaxation method to detect specific heat. For a small specimen, the relaxation method is more advantageous than the adiabatic method.

The relaxation method is illustrated in Fig. 3. The central part of the measurement technique is a chip of sapphire crystal with high purity. It is desired that this crystal has an almost zero or very weak magnetic field dependent specific heat. This crystal is hung in vacuum through several wires with low thermal conductive. On this crystal there is a Cernox thermometer and a small heater made through the micro mechanical engineering technique. They are connected to the supporting frame by the wires just mentioned above. This assembly is called as a measuring platform. The measured sample is attached to the chip by thermal conductive gel. If we send a heating power P to the platform, the temperature of the platform will satisfy the following equation:

$$C_{\text{total}}\frac{\mathrm{d}T}{\mathrm{d}t} = -K_{\text{w}}\left(T - T_{\text{cryostat}}\right) + P(t), \tag{8}$$

where C_{total} is the total specific heat of the sample and the chip, $T = T_{\text{chip}}$ is the temperature of the sample and the platform, and K_{w} is the thermal conductance of the linking wires.

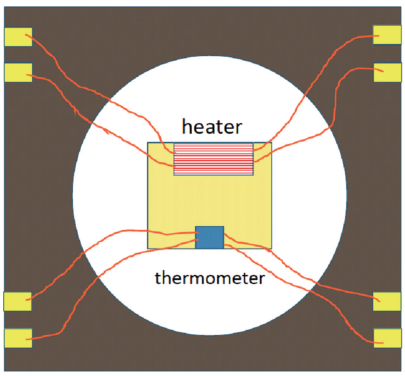


Fig. 3. The measuring platform of specific heat through the relaxation method.

The T_{cryostat} is the temperature of the supporting frame, which is normally the temperature of the base. One can see that the sample temperature is time dependent, by measuring the time dependence we can determine the total specific heat of the platform and the sample. Usually we send a rectangular-wave shaped heating power to the sample, and measure the temperature variation of the chip. Supposing the heating period starts from the moment $t = 0$, the temperature change can be written as

$$\Delta T = \Delta T_0\left(1 - \mathrm{e}^{-t/\tau}\right). \tag{9}$$

Here the relaxation constant $\tau = C_{\text{total}}/K_{\text{w}}$, ΔT_0 is the equilibrium temperature that finally reaches by the system at a long time scale, and we know that $K_{\text{w}} = \Delta P/\Delta T_0$. Through the measured data of $T(t)$, one can fit to the above equation and get the relaxation constant τ, then we can determine the total specific heat.

2.2. Different contributions to specific heat in condensed matter

In a condensed matter, there are many kinds of elementary excitations which can contribute to the specific heat in different ways. The specific heat can be written in a general way as

$$C = C_{\text{ph}} + C_{\text{el}} + C_{\text{mag}} + C_{\text{hyp}}. \tag{10}$$

Here C_{el} is the electronic contribution, C_{ph} represents the lattice vibration part, C_{mag} and C_{hyp} give the contributions of the paramagnetic centers and the nuclear moments. According to the solid state physics, the lattice vibration, or called as the phonon contribution should contribute the dominant part. The Debye model suggests that the phonon contribution in low temperature region is

$$C_{\text{ph}} \equiv \beta T^3 + \eta T^5 + \delta T^7 + \cdots \approx \frac{12\pi^4}{5} N k_{\text{B}} \left(\frac{T}{\Theta_{\text{D}}}\right)^3, \tag{11}$$

where N is the Avogadro constant, and Θ_{D} is the Debye temperature. Usually it is believed that the specific heat of phonon contribution is temperature independent. However, in some system with strong spin–lattice coupling, such as in the iron based superconductors, the situation may change.

In superconducting state, the electron distribution at different momentum will change a lot, so that the internal energy will also change. We will present the contribution to specific heat in the superconducting state in coming sections.

3. Thermodynamics about specific heat crossing $H_{c1}(T)$ and $H_{c2}(T)$

As mentioned before, a type-II superconductor has the phase transitions from the Meissner state to the mixed state at $H_{c1}(T)$ and from the mixed state to normal state at $H_{c2}(T)$. In Fig. 4, we present the schematic plot of the magnetization versus magnetic field for a type-II superconductor. Now our interests in this section are how the specific heat changes with magnetic field.

Now let us have a look at how the specific heat changes when crossing the transitions from the Meissner state to the mixed state and from the mixed state to the normal state. Suppose the Gibbs free energy in a state i is defined as

$$G_i = F_i(T, B_i)_i - B_i H_{\text{a}}. \tag{12}$$

Here F_i is the Helmholtz free energy which contains the contributions of the internal energy and entropy, and H_{a} is the external magnetic field. When the magnetic field H_{a} and temperature are constant, we need to find the optimized magnetization

of B_i in the sample through the derivative condition

$$\left(\frac{\partial G_i}{\partial B_i}\right)_{H_a,T} = 0, \quad \text{or} \quad \left(\frac{\partial F_i}{\partial B_i}\right)_{H_a,T_a} = H_a. \tag{13}$$

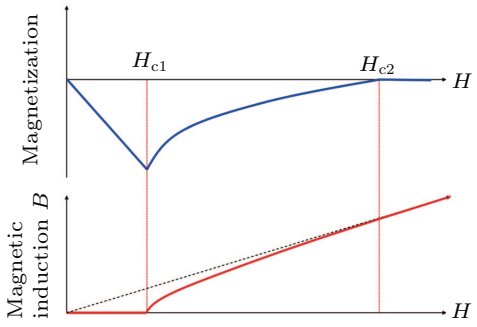


Fig. 4. Schematic plot of the magnetization and magnetic induction of an ideal type-II superconductor. The blue (red) solid line corresponds to the magnetization (magnetic induction). Blow H_{c1}, no vortices enter the superconductor. Above H_{c1}, vortices enter into the superconductor forming the mixed state. Above H_{c2}, any droplet of superconductivity will disappear, the system comes into the normal state.

Now we can get a deeper insight about the change of the Gibbs and Helmholtz free energy when crossing the two transitions. We mark the phases of the two sides of the transition with subscripts i and j. Then we can write down the following equations:

$$\frac{\mathrm{d}G_i}{\mathrm{d}T} = \frac{\mathrm{d}F_i}{\mathrm{d}T} - B_i\frac{\mathrm{d}H_{ij}}{\mathrm{d}T} - H_{ij}\frac{\mathrm{d}B_{ij}}{\mathrm{d}T} = \frac{\partial F_i}{\partial T} + \frac{\partial F_i}{\partial B_i}\frac{\mathrm{d}B_i}{\mathrm{d}T} - B_i\frac{\mathrm{d}H_{ij}}{\mathrm{d}T} - H_{ij}\frac{\mathrm{d}B_i}{\mathrm{d}T}. \tag{14}$$

Taking Eq. (13) into consideration, we see that the second and the fourth terms in the above equation will cancel each other, we thus have

$$\frac{\mathrm{d}G_i}{\mathrm{d}T} = -S_i - B_i\frac{\mathrm{d}H_{ij}}{\mathrm{d}T}. \tag{15}$$

From Fig. 4 we see that the magnetic induction B will be continuous through the two transitions. Since the value of $|\mathrm{d}H_{ij}/\mathrm{d}T|$ at the transition line will be finite, we see that the entropy of both sides will be continuous. This indicates that the transitions at either $H_{c1}(T)$ or $H_{c2}(T)$ cannot be first order. Next we try to prove that the transitions at both $H_{c1}(T)$ and $H_{c2}(T)$ are actually second order and the specific heat should have jumps. From the continuity of the entropy at both sides we have $S_i = S_j$ and $\mathrm{d}S_i/\mathrm{d}T = \mathrm{d}S_j/\mathrm{d}T$, further we have

$$\frac{\mathrm{d}S_i}{\mathrm{d}T} = \left(\frac{\partial S_i}{\partial T}\right)_{H_a} + \left(\frac{\partial S_i}{\partial H_a}\right)_T \frac{\mathrm{d}H_{ij}}{\mathrm{d}T}. \tag{16}$$

Taking the definition

$$C_i = T\left(\frac{\partial S_i}{\partial T}\right)_{H_a}, \tag{17}$$

we then can calculate the specific heat variation crossing these transitions

$$C_j - C_i = T\left(\frac{\partial S_j}{\partial T}\right)_{H_a} - T\left(\frac{\partial S_i}{\partial T}\right)_{H_a}\frac{\mathrm{d}H_{ij}(T)}{\mathrm{d}T} \times \left[\left(\frac{\partial S_j}{\partial H_a}\right)_T - \left(\frac{\partial S_i}{\partial H_a}\right)_T\right]. \tag{18}$$

Thus we have

$$C_j - C_i = \frac{\mathrm{d}H_{ij}(T)}{\mathrm{d}T}\left(\frac{\partial^2 F_{ij}}{\partial B_i \partial T}\right)\left[\left(\frac{\partial B_i}{\partial H_a}\right)_T - \left(\frac{\partial B_j}{\partial H_a}\right)_T\right]. \tag{19}$$

Considering Eq. (13), we have

$$C_j - C_i = \left(\frac{\mathrm{d}H_{ij}(T)}{\mathrm{d}T}\right)^2\left[\left(\frac{\partial B_j}{\partial H_a}\right)_T - \left(\frac{\partial B_i}{\partial H_a}\right)_T\right]. \tag{20}$$

Now we see that, since the term $|\mathrm{d}H_{ij}/\mathrm{d}T|$ is finite, while the term $(\partial B_{i,j}/\partial H_a)$ in the two sides of a transition has a sudden change, thus we expect discontinuities of specific heat at the two transitions. Near the transition of $H_{c1}(T)$, the value of $|\mathrm{d}H_{c1}(T)/\mathrm{d}T|^2$ might be small, but the change of the slope of $(\partial B_{i,j}/\partial H_a)$ is big, since the $B(H)$ curve shows a sudden rise in the mixed state. At the transition of $H_{c2}(T)$, we see that the value of $|\mathrm{d}H_{c2}(T)/\mathrm{d}T|^2$ is big, but the change of $(\partial B_{i,j}/\partial H_a)$ is small, we can also see a moderate jump down of the specific heat. We must emphasize that this can only occur in ideal type-II superconductors. In a dirty type-II superconductor, due to the vortex pinning, we may not see such effect. In Fig. 5, we show the temperature dependence of specific heat of the superconductor Nb. Two steps of specific heat can be clearly observed at $H_{c1}(T)$ and $H_{c2}(T)$.

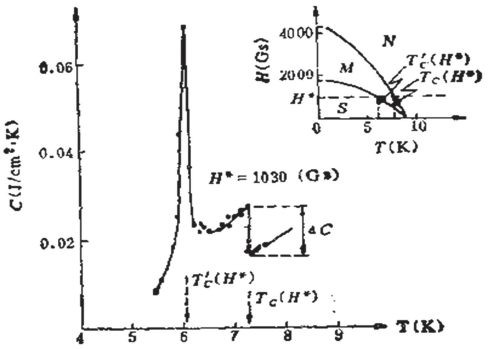


Fig. 5. Specific heat at 1030 Oe for Nb. One can see clearly the two steps at $T_{c1}(h)$ and $T_{c2}(h)$.

4. Low-energy quasiparticle excitations in mixed state and gap structure

4.1. Introduction

As we expressed above, the specific heat detects the low energy quasiparticle excitations. In a superconductor, the quasiparticles satisfy the Bogoliubov dispersion

$$E(k) = \sqrt{(\hbar^2k^2/2m - E_F)^2 + \Delta^2}. \tag{21}$$

Here $\hbar^2k^2/2m$ is the kinetic energy counting from the Fermi level. We can calculate the quasiparticle density states (DOS) in the superconducting state. It is found that the DOS is fully

gapped within the gap with singularities at the two energy gaps $\pm\Delta$ for the s-wave superconductor. In the low temperature limit, through the BCS theory, we can derive the temperature dependence of specific heat in the s-wave superconductors as

$$c_{\rm es} = 4\beta^2 k_{\rm B} \sum_{|k|>k_{\rm F}} f_k(1-f_k)(E_k^2+\beta/2{\rm d}\Delta^2/{\rm d}\beta) \propto \sqrt{T}\,{\rm e}^{-\Delta_0/kT}, \tag{22}$$

where $\beta = 1/k_{\rm B}T$, $\Delta(T)$ is the temperature dependent superconducting gap, and Δ_0 is the gap at zero temperature. One can see that in the low temperature limit, the specific heat coefficient $C_{\rm es}/T$ will be zero and it grow up gradually with increasing temperature, following a thermal activation manner.

For a d-wave superconductor, the sign of the superconducting gap changes crossing the Fermi surface and a typical gap function is $\Delta(\boldsymbol{k}) = \Delta_0 \cos 2\theta$, which is shown in Fig. 6. In cuprate superconductors, many experiments have shown that the gap has a d-wave pairing symmetry.[3] Although there is a pseudogap effect[4] which will be addressed later, experimentally, it is still shown that the condensate is constructed by Cooper pairs and the low energy physics can be described by the BCS theory. One can see that the gap has the maximum values at the four k-points $(\pm\pi, 0)$ and $(0, \pm\pi)$, which is called as the anti-nodal direction. Along the (π, π) direction, the gap is zero, which is called as the nodal direction. The specific heat actually detects the small gap region, so that the quasiparticle dispersion in a d-wave superconductor can be written as[5,6]

$$E(k) = \hbar\sqrt{v_{\rm F}^2 k_\perp^2 + v_\Delta^2 k_\parallel^2}. \tag{23}$$

Here $\hbar$ is the Planck constant, $v_{\rm F}$ is the Fermi velocity which reflects the dispersion in the direction $(k_\perp)$ perpendicular to the Fermi surface, while v_Δ is the gap slope around the nodal point, which reads as

$$v_\Delta = \left.\frac{{\rm d}\Delta}{{\rm d}\theta}\right|_{\rm node} \frac{1}{\hbar k_{\rm F}}, \tag{24}$$

and reflects the dispersion parallel to the Fermi surface $(k_\parallel)$.[7] This dispersion naturally leads to a linear relation between the DOS and energy near zero energy, which reads as

$$N_{\rm s}(E) = \frac{2}{\pi\hbar^2}\frac{1}{v_{\rm F}v_\Delta}E. \tag{25}$$

The DOS for the s-wave and d-wave superconductors is shown in Fig. 7. In the clean limit, the low temperature specific heat of an s-wave superconductor will be zero. While for a d-wave superconductor, the specific heat is described by a quadratic temperature dependence[7,8]

$$C_{\rm el}(T) = \alpha T^2 = A\frac{k_{\rm B}^3}{\hbar^2}\left(\frac{1}{v_{\rm F}v_\Delta}\right)T^2. \tag{26}$$

Here A is a constant which concerns the detailed atomic structure of the material, and $k_{\rm B}$ is the Boltzmann constant. This quadratic temperature dependence for a d-wave superconductor is in sharp contrast with that of a conventional superconductor which shows an exponential temperature dependence in the low temperature region. If temperature is increased, some quasiparticles will be generated immediately. For an s-wave superconductor, this excitation process is very slow versus temperature. For a d-wave superconductor, the quasiparticle DOS will be[7]

$$\frac{N_n(T)}{m} = \frac{2\ln 2}{\pi}\frac{k_{\rm B}}{\hbar^2}\frac{n}{d}\alpha_{\rm FL}^2\left(\frac{v_{\rm F}}{v_\Delta}\right)T. \tag{27}$$

Here m is the mass of the charge carrier, $\alpha_{\rm FL}$ is the correction factor of the Fermi liquid, in the order of unity, and d is the distance between the double CuO planes in one unit cell of the cuprate superconductor. By measuring the low temperature penetration depth or the superfluid density, one can also determine the gap structure. For a d-wave superconductor, $\Delta\lambda(T)$ will increase with T linearly, while for an s-wave superconductor, the penetration depth will increase with T in an exponential way.

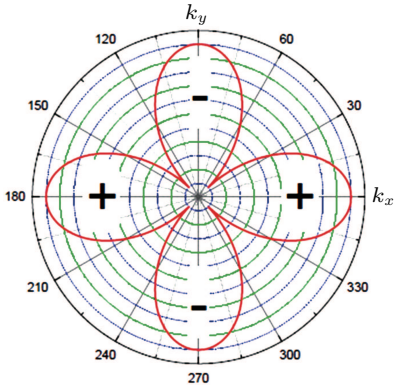


Fig. 6. The d-wave superconducting gap (Δ/Δ_0) in the momentum space. Here the sign '+' and '−' indicates the opposite phase of the gap.

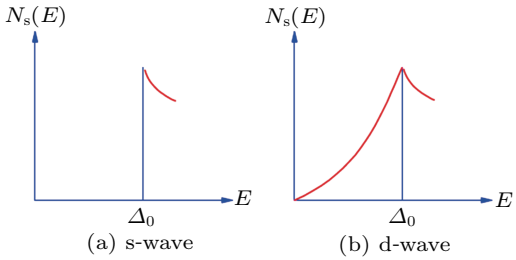


Fig. 7. The density of states for (a) s-wave and (b) d-wave superconductors.

4.2. Specific heat under magnetic fields

For a type-II superconductor, when the external magnetic field is larger than the lower critical value $H_{\rm c1}$, the magnetic flux will penetrate into the superconductor to form vortices. For a vortex, it contains a core region with the size of about the coherence length ξ. Solving the Ginzburg–Landau equation

around a vortex would give the distribution of the supercurrent density $\boldsymbol{j}(r)$ and magnetic induction $\boldsymbol{B}(r)$, and the order parameter $|\Psi(r)|$. It is known that $\boldsymbol{j}(r)$ and $\boldsymbol{B}(r)$ will change in a scale of the penetration depth $\lambda_{\rm L}$, while the order parameter will change in the scale of the coherence length ξ. For the vortex system, we have two contributions from the low energy quasiparticles.

The first contribution comes from the finite density of states within the vortex cores. By solving the Bogoliubov–de Gennes equations, researchers find that the gap value actually changes spatially with the cylindrical space of 2ξ.[9] Detailed calculation shows that there are some quantized levels[9,10] of these states with the energies of $\varepsilon_n \approx \pm n/2\Delta_0^2/E_{\rm F}$ ($n = 1, 3, 5$), and the energy discretion is about $\varepsilon_0 \approx \pm\Delta_0^2/E_{\rm F}$. For example, the lowest level is $\varepsilon_1 \approx \pm 1/2\Delta_0^2/E_{\rm F}$. Here $E_{\rm F}$ is the Fermi energy, and Δ_0 is the superconducting gap. In conventional superconductors, $E_{\rm F} \gg \Delta_0$, the discretion between the energy levels is very small and very difficult to be observed. At the meantime, the measuring temperature is usually much larger than the energy discretion between different levels. This leads to a continuum spectrum of DOS near zero energy.[11] This is just the origin of the usually observed zero energy peak within the vortex cores.[12] For a single vortex, this contributes almost a constant to the total density of states. In Fig. 8, we show a series of STM spectra[12] of a vortex core in 2H-$NbSe_2$. One can see that there is a high density of state peak at zero energy contributed by this vortex.

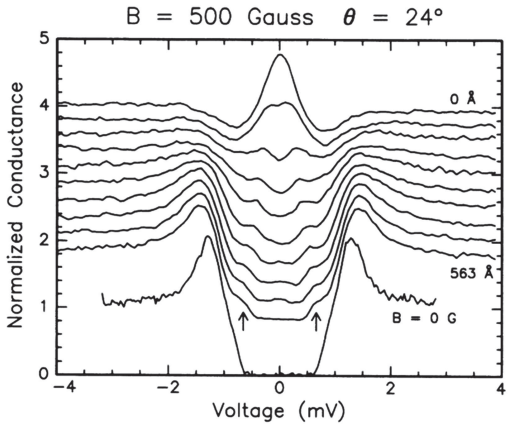


Fig. 8. Scanning tunneling spectrum with a vortex core in 2H-$NbSe_2$. Figure from Ref. [12]. APS Copyright.

By increasing the magnetic field, the total contribution to specific heat of the vortex core part is just proportional to the density of vortices. We thus expect a linear relation of this part

$$C_{\rm el}^{\rm s-wave}(T,H) = \gamma(H)T = \gamma_n \frac{H}{H_{\rm c2}} T. \tag{28}$$

The second contribution would come from the outside core of the vortices, mainly in the region of $\lambda > r > \xi$. In this part, the superconducting current is flowing but the order parameter has already established. The low energy quasiparticle excitations would be the same as in Meissner state if there would be no supercurrent. So the supercurrent will add a momentum to each Cooper pair. That is to say, the kinetic energy of the condensate will be shifted by a small amount due to this effect, and thus the contribution of DOS will also change. This is called as the Doppler effect. This extended density of states was first mentioned theoretically by Volovik.[13] This little shift energy is $\delta E(\boldsymbol{k}) = \boldsymbol{v}_{\rm s} \cdot \hbar\boldsymbol{k}$ with $\boldsymbol{v}_{\rm s}$ the velocity of the superfluid. A calculation in the region of $r > \xi$ shows that the superfluid velocity can be approximated as $|\boldsymbol{v}_{\rm s}| = \hbar/2mr$ with m the electron mass and r the distance to the center of the vortex core. For a single vortex, the contribution is about

$$N_{\rm single} \propto \int_{\xi}^{R} v_{\rm s} 2\pi r {\rm d}r. \tag{29}$$

Input the relation $|\boldsymbol{v}_{\rm s}| = \hbar/2mr$ to the above equation, we have $N_{\rm single} \propto R$, combining with $R = \sqrt{\Phi_0/2\pi H}$ (when $H_{\rm c2} \gg H \gg H_{\rm c1}$), we have $N_{\rm single} \propto 1/\sqrt{H}$. Since the vortex density is proportional to H, thus we have

$$C_{\rm el}(T,H) = \gamma(H)T = \gamma_n \sqrt{\frac{8}{\pi}} a \sqrt{\frac{H}{H_{\rm c2}}} T = A\sqrt{H}. \tag{30}$$

This is the well-known Volovik relation[13] for a d-wave superconductor. Here a is a vortex-structure factor which is close to 1, the pre-factor $A \propto 1/v_\Delta \propto 1/\Delta_0$ with Δ_0 the maximum d-wave gap.[7,8,14]

4.3. Scaling law of specific heat in mixed state

Strictly speaking, the Volovik effect mentioned above, namely, $C_{\rm el} \propto \sqrt{H}T$ works only for $T/\sqrt{H} \ll T_{\rm c}/\sqrt{H_{\rm c2}}$. Under other circumstances, for example, when $T/\sqrt{H} > T_{\rm c}/\sqrt{H_{\rm c2}}$, the electronic specific heat $C_{\rm el}(T,H)$ will contain a T^2 term which is independent of the magnetic field and an H linear term.[15] To cover a wider situation, Simon and Lee[16] pointed out that in much wider magnetic field H and temperature region, the specific heat may have a scaling law

$$\frac{C_{\rm el}(T,H)}{T\sqrt{H}} = F\left(\frac{T}{\sqrt{H}}\right), \tag{31}$$

where $F(x)$ is a scaling function. Up to now, there is no precise expression of $F(x)$. However some empirical laws have been found,

$$\frac{C_{\rm el}(T,H)}{T\sqrt{H}} = Af(y), \quad f(y) = \frac{1}{1+y}, \quad y = \eta\sqrt{\frac{H_{\rm c2}}{H}}\frac{T}{T_{\rm c}}. \tag{32}$$

Here η is close to unity.[17] When $y \ll 1$ (namely, in low temperature and high magnetic field), $f(y) \to 1$, the above scaling law recovers the Volovik relation $\frac{C_{\rm el}(T,H)}{T} = A\sqrt{H}$. When $y \gg 1$ (in the high field region), we have $f(y) \to 1/y$, the above scaling relation corresponds to the case of a linear H term.

4.4. Impurity scattering effect in d-wave superconductor

In the above section, we have discussed about the low energy quasiparticle excitations in the clean limit, which in practical is not the case. In a real material, we cannot avoid the existence of defects, disorders, and impurities. These will have strong influence on the DOS excitation in the materials, especially for superconductors with nodes. In the dirty limit, namely, the mean free path is comparable to the coherence length, the small gap amplitude near nodes will be strongly suppressed and lead to the excitations of quasiparticles, leading to the clear deviation from the ideal clean limit.[18] Taking this effect into account, Kübert *et al.* calculated the specific heat at $T = 0$, the magnetic field induced specific heat $C_{\rm el}(T,H) = \gamma(H)T$ and find that it is clearly deviated from the Volovik relation and satisfies the $H\log H$ law[18]

$$\frac{\gamma(H)}{\gamma_n} \cong \frac{\Delta_0}{8\gamma_0} a^2 \left(\frac{H}{H_{c2}}\right) \log\left[\frac{\pi}{2a^2}\left(\frac{H_{c2}}{H}\right)\right], \tag{33}$$

where γ_0 is the de-pairing factor which depends on the scattering potential.

However, the above relation has not been confirmed by experiment. In most cases, the Volovik relation seems to be obeyed very well.[7,8,19,20] The further theoretical advances show that the strong correlation effect may play an important role here.[21] In Fig. 9, we show the calculated DOS versus energy by Garg *et al.*[21] with different scattering density with the strong correlation effect (a) considered and (b) not considered. One can see that, with the strong correlation effect considered, the low energy quasiparticle density of states does not enhance with the impurity density too much. It seems that the gap near the nodes is somehow protected by the strong correlation effect. This explains why in the cuprate, with a lot of dopants, the predicted Volovik relation for a clean d-wave superconductor can still be observed.

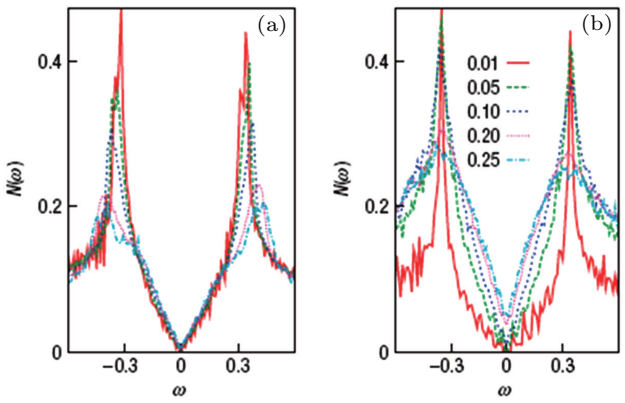


Fig. 9. Density of states versus energy with the strong correlation effect considered (a) and not considered (b) under different impurity densities. The figure is copied from Ref. [21]. Copyright Nature Publishing Company.

5. Specific heat investigation of cuprate superconductors

5.1. Introduction to pseudogap and Fermi arc state in cuprates

Although the cuprate superconductivity has been discovered for 30 years, about the superconductivity mechanism, no consensus has been reached. However, in the process of research, some important progresses or new phenomena have been observed. Among them are (1) recognition of d-wave pairing symmetry,[3] (2) pseudogap state above T_c,[4] and (3) Fermi arc state[22–25] or pocket state. These features are quite different from the conventional superconductor. Let us have a look one by one.

5.1.1. The d-wave pairing symmetry in cuprates

It becomes more and more clear that, the order parameter in cuprates is described by the d-wave gap function

$$\Delta_{\rm d} = \Delta_0(\cos k_x - \cos k_y). \tag{34}$$

Along the Fermi surface, supposing to be an isotropic circle like, namely, $k_x^2 + k_y^2 = (\pi/a)^2$, we can see that the d-wave gap takes the maximum along $(\pm\pi, 0)$ and $(0, \pm\pi)$. These directions are called as the anti-nodal direction. The diagonal direction, namely, the (π, π) direction and its equivalent symmetric directions are called as the nodal direction. Since the gap function will be zero at the crossing point of this direction and the Fermi surface. In Fig. 10, we show the Fermi surface, the gap function is shown in Fig. 6 in a schematically way. This d-wave has been well proved by angle resolved photoemission spectroscopy (ARPES),[26,27] phase sensitive experiment,[3] thermal conductivity,[28] and specific heat.[7,8,19,20]

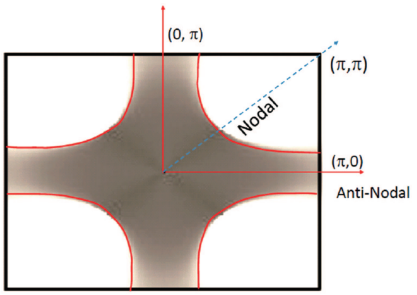


Fig. 10. Schematic plot of Fermi surface in cuprate. The Fermi surface is highlighted by the solid red line around the BZ center. In underdoped region, this Fermi surface is truncated, showing only the segment or pocket near the nodal point.

5.1.2. Pseudogap

In the framework of BCS theory, the gap will be established at the momentum of locus of the Fermi surface just below T_c. The gapping to the electrons occurs simultaneously crossing all Fermi surface and the long range order of superconductivity is established. In the cuprate superconductors, the NMR data show that the spin relaxation rate starts

to drop at a temperature far above T_c.[29] Later ARPES data show the gapping near the anti-nodal direction at temperatures far above T_c.[26,27] This is certainly beyond the understanding of the BCS picture. This effect is called as the pseudogap feature,[4] manifesting itself that the gap is not like the well established gap in the superconducting state. This effect was later also found from the measurements of tunneling spectrum,[30] deferential specific heat,[31] resistivity, etc. The pseudogap temperature is denoted by T^*. So far the pseudogap feature has not got a complete understanding yet, and we do not know whether it is related to superconductivity or it is just a new phase which competes with superconductivity. In recent years, many experiments point out that one of the candidates for the pseudogap would be the electronically induced charge density wave gap. This is however perhaps only part of the story. Since this exceeds the scope of this paper, we will omit this part.

5.1.3. Fermi arc

As we addressed above, in cuprate superconductors, the gapping process occurs near $(\pi, 0)$ at temperatures far above T_c, leading to the formation of pseudogap. Later, ARPES data find that the emergent Fermi surface by increasing temperature is constructed by just segments, that is, the Fermi surface is incomplete and not continuous.[16,32] The question relies whether the normal state has a truncated Fermi surface. Refined ARPES measurements with variable temperatures show that the Fermi surface shows Fermi arcs near the nodal point. Upon increasing temperature, the Fermi arcs extend to longer length and finally may connect into a complete closed Fermi surface.[23–25] Researchers also find that, by increasing the doping level, the Fermi arc length is getting longer and longer at temperatures just above T_c. This truncated normal state Fermi surface will become complete at the doping level of around 0.19–0.20, indicating a quantum critical point.[32] If the normal state shows the Fermi arc like Fermi surface, it is interesting to know how the superconducting gap is established on these Fermi arcs. We have done systematic measurements of specific heat and find that the superconducting condensation process may be understood in the following picture. Figure 11 shows the cartoon picture.

In this Fermi arc picture, the central pairing strength is determined by the gap slope, namely, v_Δ. In an ideal d-wave superconductor, the maximum gap Δ_0 is proportional to the superconducting transition temperature. While in cuprate superconductors, the anti-nodal area is gapped away, therefore it is difficult to associate the maximum gap Δ_0 with T_c. Wen *et al.*[7,8] made the detailed measurement on the low energy quasiparticle excitations in wide doping regime and found that the gap slope will increase towards underdoping level. The superconducting transition temperature T_c is however roughly proportional to the gap energy at the terminals. We will discuss this in the coming sections.

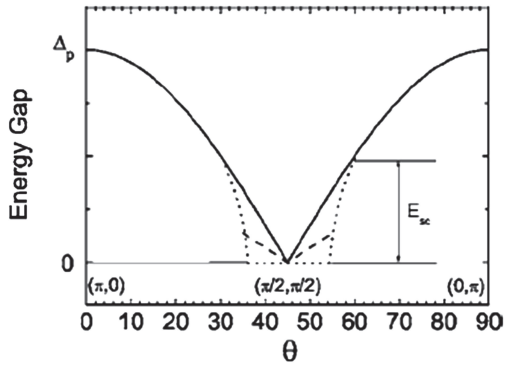


Fig. 11. Superconducting gap established on the Fermi arcs near the nodal point $(\pi/2, \pi/2)$. The solid line represents the standard d-wave gap function $\Delta = \Delta_0 \cos 2\theta$, while the dashed and dotted lines show the cases for a real superconducting gap established on the Fermi arc near the nodal point. The superconducting gaps are determined by the value at the terminals of the Fermi arc.

5.2. Bulk evidence of d-wave pairing in $La_{2-x}Sr_xCuO_4$

In the past 20 years, the d-wave superconducting gap symmetry has been well proved by many experimental tools. This includes the ARPES[26,27] and the phase sensitive experiment.[3] However, all these experiments are done by using surface tools which are very sensitive to the surface state, therefore bulk evidence is strongly needed. Specific heat can detect the bulk properties of the order parameter, and it contribute important information about the electronic states near the Fermi energy, therefore it is quite useful.

As we have addressed previously, for a d-wave superconductor, when the magnetic field is zero, the low energy quasi-particle excitations can be linear with energy, therefore the electronic specific heat will exhibit a power law behavior $C_{\rm el}(T) = \alpha T^2$. When a magnetic field is applied, the Doppler shift effect of the superconducting condensate outside the vortex core will lead to extra quasiparticle excitations, leading to a linear term $C_{\rm el}(T,H) = A\sqrt{H}T$. In the experiment, the quadratic term αT^2 at zero field and the linear term $A\sqrt{H}T$ at finite magnetic fields have been observed in YBCO by Moler *et al.*[20] In determining the quadratic term αT^2, there have been some controversy, because this term behaves as a combination of a linear term $\gamma_0 T$ and a phonon term βT^3. In fitting to the experimental data, it was found that the value of α may be negative, which is not reasonable. Theoretical estimate tells that $\alpha \sim \gamma_n/T_c$, which is a very small value in the low temperature region. Many groups have done careful experiments on low temperature specific heat.[7,8,24,33–40] It seems quite difficult to detect or determine this term αT^2 precisely.

In experiments of YBCO and $La_{2-x}Sr_xCuO_4$ (LSCO), it was found that the Doppler shift induced enhancement of specific heat $A\sqrt{H}T$ is more easy to be determined since it is purely a magnetic field induced contribution. For YBCO,

several groups derived the $A\sqrt{HT}$ term, and the pre-factor A they obtained was also consistent with each other. Later the group in Geneva determined the $A\sqrt{HT}$ term in a slightly overdoped YBCO, and calculated several important quantities, such as v_Δ, H_{c2}, and ξ, which were close to the values determined from other experiments.[33] For LSCO, the situation is similar, several groups investigated the specific heat under magnetic field and derived the term $A\sqrt{HT}$.[7,8,39] The group in Tokyo investigated low temperature specific heat in LSCO single crystals under different magnetic fields.[39] They concluded that for overdoped sample $p = 0.19$, the results obeyed the d-wave predictions, namely, the $\sqrt{HT}$ relationship, while in optimally doped sample $p = 0.16$ and underdoped sample $p = 0.10$, they claimed that it was in the dirty limit, that is, $\gamma(H) \propto H \log H$. Actually this group used the formula $[C(T,H \parallel c) - C(T,H \parallel ab)]/T$ to derive the $\gamma(H)$ term, they used the $C(T,H||ab)$ as the background contribution including the phonon and electronic contributions at zero field, which is certainly imprecise since the term $C(T,H||ab)$ may also have the contributions of low energy quasiparticle by vortices when the magnetic field is parallel to the *ab*-plane.

For a d-wave superconductor, we have shown that there is a scaling law $C_{el}(T,H)/T\sqrt{H} = F\left(T/\sqrt{H}\right)$, which has been well proved in some YBCO and LSCO samples.[7,8,20,32–40] This consistency with the Volovik relation $\Delta\gamma = A\sqrt{H}$ acts as a proof of the d-wave pairing symmetry.

We have also done a systematic investigation on LSCO single crystal samples. The advantage of this system is that the doping level can be easily tuned through the substitution of La by Sr. Comparing with the YBCO system, it is found that the LSCO system has rather weak Schotky anomaly,[7,8] this significantly lowers down the uncertainty of the data analysis. In Fig. 12 we present the magnetic field enhanced specific heat versus magnetic field.

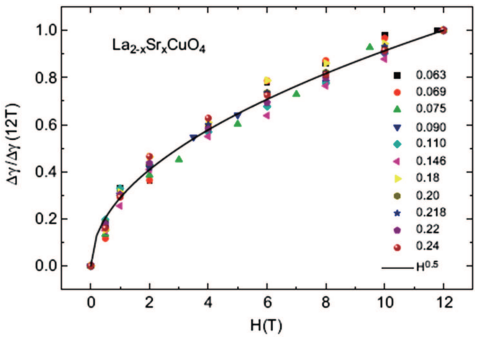


Fig. 12. Magnetic field induced enhancement of specific heat coefficient.[7,8,14] The experimental data are the values derived through the extrapolation to lower temperatures and normalized by the value at 12 T. The solid line is a theoretical fitting to the Volovik relation $\Delta\gamma(T \to 0) = \gamma(H) = A\sqrt{H}$.

One can see that the data cover a very wide region, from very under doped to very overdoped region.[7,8] The vertical coordinate shows the normalized value of $\Delta\gamma = [C(H) - C(0)]/T$ at 12 T. The solid line is a theoretical fitting to the data by the Volovik relation, but clearly the A is doping level dependent. Actually this A value relies on the gap slope near the nodal point. Next we derive the gap slope near the nodes. From the scaling, we can get the doping dependence of the pre-factor A. For a 2D superconductor, assuming that the c-axis lattice constant is l_c, the number of conducting layers is n in one unit cell, we have[41]

$$A = \alpha_p \frac{4k_B^2}{3\hbar l_c}\sqrt{\frac{\pi}{\Phi_0}}\frac{nV_{mol}}{v_\Delta}. \tag{35}$$

For LSCO, $l_c = 13.28$ Å, $V_{mol} = 58$ cm^3/mol (the volume per mol), α_p is a dimensionless constant taking 0.5 (0.465) for a square (triangle) vortex lattice, $n = 2$ (the number of Cu–O planes in one unit cell), and Φ_0 is the flux quanta. The doping dependence of A and the calculated gap slope v_Δ are shown in Fig. 13. Shown together is the normal state specific heat coefficient γ_n determined from Hall effect measurements.[42]

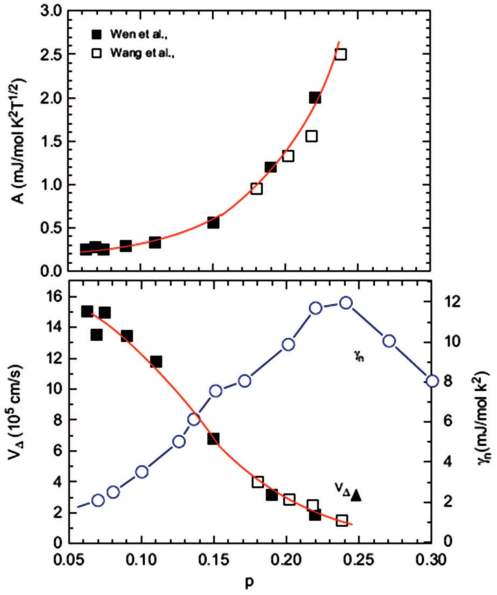


Fig. 13. (a) The pre-factor A of the Doppler shift effect and (b) the gap slope v_Δ derived by using Eq. (36). Shown in (b) by circle symbols are the normal state specific heat coefficient γ_n.

From Fig. 13 we can see that the gap slope v_Δ increases monotonically towards underdoping. This is in sharp contrast with the decreasing of the superconducting temperature in the underdoped side. Actually the doping dependence of the gap slope follows the similar way of the pseudogap or the pseudogap temperature.[4] To illustrate this more clearly, we show in Fig. 13 the doping dependence of v_Δ and T^*. The pseudogap temperature T^* here is obtained from Ref. [4], which is determined from the resistivity or spin susceptibility measurement. It is thus quite clear that the doping dependences of v_Δ and T^* are quite similar. According to the d-wave formula $\Delta(k) = \Delta_0 \cos 2\theta$, we can relate the gap slope v_Δ with the maximum gap Δ_0 at the anti-nodal point as

$$\Delta_0 = \frac{1}{2}\hbar k_F v_\Delta. \tag{36}$$

Here k_F is the Fermi vector at the nodal point (π /2, π /2). From the ARPES data, we get $k_F \cong 0.7$ Å^{-1} which is almost doping independent. Therefore we can calculate the maximum gap at the momentum point (π, 0) based on the nodal gap slope v_Δ and show them in Fig. 14.

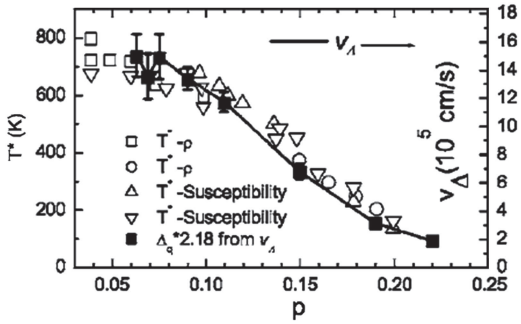


Fig. 14. Doping dependence of the maximum gap at (π, 0) (filled points) based on the nodal gap slope v_Δ and the pseudogap temperature T^* (open symbols). The pseudogap temperature T^* was taken from Ref. [4], which was determined from the resistivity and spin susceptibility measurements.

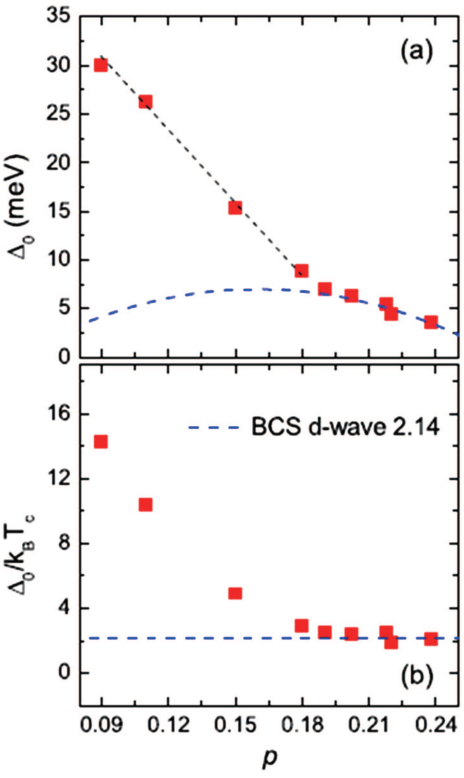


Fig. 15. (a) Doping dependence of the maximum gap Δ_0 in the d-wave gap function derived from the nodal gap slope v_Δ. The blue dashed line shows the doping dependence of the maximum gap of the d-wave gap. (b) The ratio between the obtained maximum gap and T_c. In the overdoped region, it gradually approaches the d-wave ratio $\Delta_0 \cong 2.14 k_B T_c$.[19] Below $p = 0.19$, the derived Δ_0 clearly deviates from the theoretical prediction and goes up towards underdoping.

The doping dependence of the maximum gap derived from the data of v_Δ is shown in Fig. 15. We can see that in the doping regime $p \leqslant 0.19$, there is a simple linear correlation between Δ_0 (denoted here as Δ_q) and T^*, namely, $\Delta_q \sim 0.46 k_B T^*$. This is in sharp contrast with the really measured superconducting transition temperature T_c.[7] This may suggest that the maximum gap has a close relation with the pseudogap. Through analyzing the thermal conductivity in the underdoped region, the group in Canada[28] has derived the similar conclusion. One cannot use the maximum gap Δ_0 to derive the superconducting transition temperature. When $p \geqslant 0.19$, the derived Δ_0 has a similar doping dependence with T_c and surprisingly the d-wave relation $\Delta_0 \cong 2.14 k_B T_c$ is well satisfied. This is also consistent with other experiments.[43,44]

5.3. Pseudoap and Fermi arc state in cuprate

ARPES measurements show that the detected Fermi surface is not complete, but rather segment like.[32] The Fermi surface appearing first is the locus of the nodal point ($\pi/2$, $\pi/2$) and it extends to anti-nodal direction. Therefore it is called as the Fermi arc state. The superconducting gap detected by specific heat gives the gap slope v_Δ which in usual case reflects the pairing strength. Our experiment shows that the gap slope increases towards underdoping, which may indicate that the pairing strength gets enhanced towards underdoping. However, we know that the superconducting transition temperature drops down towards underdoping. The opposite doping dependence of v_Δ and T_c tells that the superconducting transition temperature in the underdoped region may not just depend on the pairing strength, but also some other effect. We believe that it should have close relation with the Fermi arc state in the underdoped region. In the underdoped region, just above T_c the Fermi surfaces are constructed by the segments of Fermi arcs near the nodal point, while in the overdoped region, at the doping level of about $p = 0.19$, the Fermi surface suddenly becomes a complete one.[42] Based on the specific heat data, we believe that the ground state when superconductivity is completely suppressed by the magnetic field is the Fermi arc state,[41] in this case the charge carrier density is proportional to the hole number, namely, $n_s \propto p$, while in the overdoped region the Fermi surface becomes complete, the charge carriers become electron like and the charge carrier number becomes $n_s \propto 1 + p$.[42] Concerning the underdoped electronic state, there are two different views: one picture assumes that the ground state will be a nodal metal state, which means that a nodal metal will be recovered when the superconductivity is suppressed by the magnetic field, the other view assumes that the recovered normal state will be a Fermi arc state. The two cases are shown below in view of specific heat. In the picture of Fermi arc, a finite DOS will appear when the superconductivity is killed completely.

In order to check whether it is a Fermi arc ground state or a nodal metal state, we have measured the specific heat for a very underdoped sample $La_{2-x}Sr_xCuO_4$ ($x = 0.06$). After deducting the phonon contribution we present the magnetic field induced electronic specific heat in the zero temperature limit. One can see that with the increase of magnetic field, more and

more density of states are recovered and the electronic specific coefficient increases. We further find that this enhanced part is roughly described by the Volovik relation for a d-wave superconductor, that is, $\Delta\gamma = A\sqrt{H}$. Therefore our data strongly supports the Fermi arc picture and the superconducting gap is built up upon the Fermi arc near nodes.

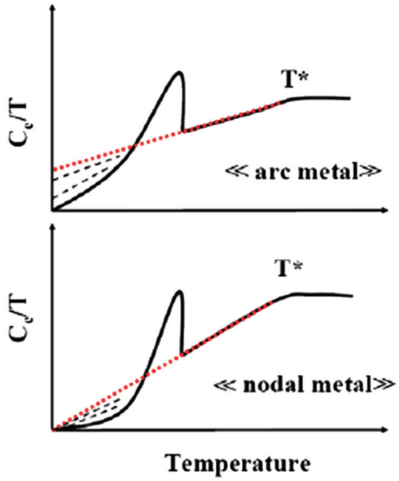


Fig. 16. A schematic plot for the electronic specific heat when superconductivity is killed completely. (a) Fermi arc picture, a finite electronic specific heat coefficient will be detected in zero temperature limit. (b) Nodal metal picture, there is no finite density of states at the zero temperature limit. T^* here is the pseudogap temperature which can be detected from differential specific heat and resistivity.[45]

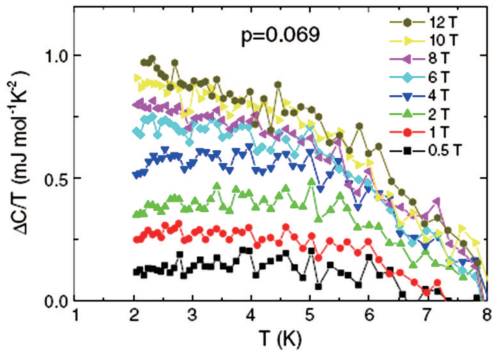


Fig. 17. The specific heat at different magnetic fields subtracted by that at zero field for a typical underdoped LSCO single crystal $p = 0.069$.[7] The figure is copied from Ref. [7], APS copyright.

5.4. Superconducting condensation based on the Fermi arc picture

We have argued that the ground state of the underdoped cuprates is the Fermi arc metal. Now we show how the superconducting condensation is established based on the Fermi arc picture. From the above discussion we know that the slope of the superconducting gap v_Δ near the nodal point has been measured through our specific heat measurement. This nodal gap slope v_Δ reflects actually the pairing strength. The similar doping dependence of T^* and v_Δ hinges on the intimate relation between superconductivity and pseudogap. Then the question is why the superconducting transition temperature drops down in the underdoped region. Here based on the phase coherence picture we propose the superconducting gapping on the Fermi arcs to understand the superconducting transition.

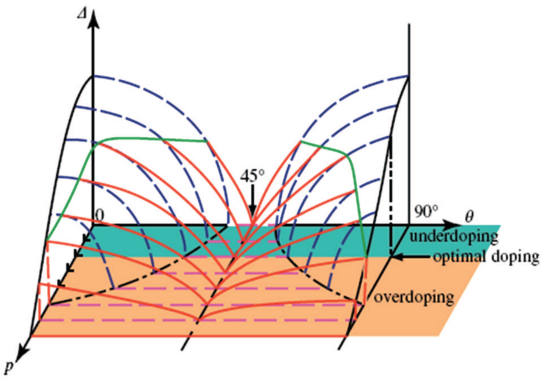


Fig. 18. The schematic picture for the superconducting condensation based on the Fermi arc picture. We now extend the momentum angle from 0 to $\pi/2$, corresponding to the momentum from $(\pi, 0)$ to $(0, \pi)$. The two terminals are corresponding to the anti-nodal points with the maximum gap. While at the angle of 45° it is at the nodal point with zero gap. For an underdoped sample, the length of the Fermi arc is finite and is highlighted by the horizontal dashed line. With more doping, this Fermi arc length becomes longer and longer. Below T_c, a superconducting gap will be formed on these Fermi arcs. This figure is adopted from Refs. [7,8]. The dashed blue line represents the pseudogap. The green solid line shows the energy scales on the terminals of the Fermi arcs.

In the conventional BCS superconductor, the pairing strength or the gap is related to the DOS at Fermi energy (N_F) through $\Delta = 2\hbar\omega_D \exp(-1/N_F\lambda)$, with ω_D the Debye frequency and λ the electron–phonon coupling strength. Clearly, this formula cannot be used to describe superconductivity in the underdoped region. We have determined the gap slope v_Δ near the nodal point. In the Fermi arc state, the effective DOS at the Fermi energy is significantly suppressed by the pseudogap effect. However, we have the energy at the terminals of the Fermi arc, as highlighted by the green solid lines in Fig. 18. Now we can calculate this energy and compare it with the superconducting transition temperature T_c.

In a normal metal, the electronic specific heat coefficient is $\gamma_n = \frac{\pi^2}{3}k_B^2 N_F V_{mol}$. In the underdoped region, the effective DOS will be determined by the length of the Fermi arcs. Supposing the Fermi arc length is k_{arc} and we assume that the DOS on the Fermi arc is uniform, then we can imagine that $N(E_F) \propto k_{arc}$. Detailed calculation[41] gives $N(E_F) = \frac{2nk_{arc}}{\pi^2\hbar d v_F}$. Therefore the normal state specific coefficient can be written as

$$\gamma_n(0) = \frac{2k_B^2}{3\hbar}\frac{n}{d}\frac{V_{mol}}{v_F}k_{arc}. \tag{37}$$

With the increase of doping level p, the Fermi arc length k_{arc} increases linearly, which enhances $\gamma_n(0)$. When it comes to the overdoped region, the Fermi surface becomes complete, the effective $\gamma_n(0)$ will not increase with the doping level. In the inset of Fig. 19, we show the doping dependence of the effective specific heat coefficient $\gamma_n(0)$ of the LSCO system

dtermined from the specific hea measurements, and also converted from the integrated photoemission spectroscopy measurements and NMR measurements.[41] In the doping region $p \leqslant 0.2$, it is clear that $\gamma_n(0)$ increases linearly with p. In the region $p > 0.2$, the $\gamma_n(0)$ tends to be stable versus doping.

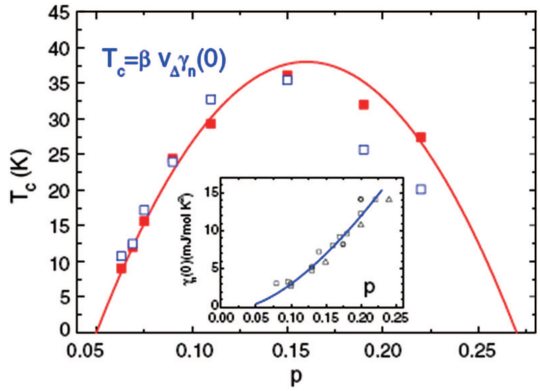


Fig. 19. Doping dependence of the measured superconducting transition temperature T_c (solid symbols) of the LSCO system and the calculated T_c based on the Fermi arc model (open symbols).[6,39] The solid line is the empiric relation[47] $T_c/T_c^{\max} = 1 - 82.6(p-0.16)^2$, where $T_c^{\max} = 38$ K. The inset presents the normal state specific coefficient in the zero temperature limit $\gamma_n(0)$ adopted from Ref. [46]. The solid line in the inset shows a fit to the data with $\gamma_n(0) = \zeta(p-p_c)^\eta$ with $\zeta = 182.6$, $p_c = 0.03$, and $\eta = 1.54$.

Now we try to calculate the energy at the terminals of the Fermi arc. We assume an energy scale Δ_{sc} which governs the superconducting transition temperature T_c. We can imagine that this energy scale is proportional to both the gap slope v_Δ and the Fermi arc length k_{arc}, thus we have

$$\Delta_{sc} \propto v_\Delta \gamma_n(0). \tag{38}$$

For a more precise calculation, we have $\Delta_{sc} \cong \frac{1}{2} v_\Delta \hbar k_{arc}$. Using Eq. (38) we further have

$$T_c = \frac{3\hbar^2}{8.56 k_B^3} \frac{d}{n} \frac{v_F}{V_{mol}} v_\Delta \gamma_n(0) = \beta v_\Delta \gamma_n(0). \tag{39}$$

From the above equation, we immediately understand why the superconducting transition temperature T_c drops down in the underdoped region, this is because the Fermi arc length becomes shorter towards underdoping, this is reflected from the decrease of $\gamma_n(0)$. Although the gap slope v_Δ or the maximum gap Δ_0 increases towards underdoping, the superconducting energy scale or transition temperature is determined by the multiplication of the gap slope and the Fermi arc length. The calculated T_c is presented in Fig. 19 by the open symbols, the really measured T_c is shown by the filled symbols. In the calculation of the superconducting energy scale, we have fitted the doping dependence of $\gamma_n(0)$ with a relation $\gamma_n(0) = \zeta(p-p_c)^\eta$, the fitting yields $\zeta = 182.6$, $p_c = 0.03$, and $\eta = 1.54$. In the underdoped side, both sets of data consist with each other very well. In the overdoped region, the calculated data are deviating from the experimental values, this is understandable since the fitted relation of $\gamma_n(0)$ cannot be used anymore. In the heavily overdoped region, there might be electronic phase separation or the strong pair breaking by the impurity effect.

6. Iron based superconductors

Since the discovery of iron based superconductivity in 2008, many systems have been discovered.[48,49] In iron based superconductors, specific heat measurements have been done in plenty material systems,[50–55] all showing the multigap feature. For a multiband system, we normally fit the temperature dependence of electronic specific heat using the linear combination of multiple terms, each has a gap structure. The specific heat formula reads as

$$\gamma_e = \frac{4N_F}{k_B T^3} \int_0^{+\infty} \int_0^{2\pi} \frac{e^{\varsigma/k_B T}}{(1+e^{\varsigma/k_B T})^2} \times \left[\varepsilon^2 + \Delta^2(\theta,T) - \frac{T}{2}\frac{d\Delta^2(\theta,T)}{dT}\right] d\theta d\varepsilon. \tag{40}$$

Here $\varsigma = \sqrt{\varepsilon^2 + \Delta^2(T,\theta)}$, the gap anisotropy is included in the function $\Delta(T,\theta)$, the temperature dependence is assumed to be the BCS like, and $\varepsilon = \hbar^2 k^2/2m$ is the kinetic energy of electrons. Usually, we fit the data at zero magnetic field, then use the magnetic field to suppress superconductivity and to observe the magnetic field dependence of the extra DOS. In this way, we can judge roughly the anisotropy of the gap and the gap magnitude. In the following, we will introduce the specific heat investigation in several systems, including $Ba_{0.6}K_{0.4}Fe_2As_2$,[51] $BaFe_{2-x}Co_xAs_2$,[52] and FeSe bulk.[55]

6.1. Specific heat investigation on $Ba_{0.6}K_{0.2}Fe_2As_2$

The $Ba_{0.6}$ $K_{0.2}Fe_2As_2$ system has been found to contain multiband by ARPES[56] and STM[57] in very early date. In Fig. 20, we show the raw data of specific heat in two optimally doped $Ba_{0.6}K_{0.2}Fe_2As_2$ samples. One can see several important facts. (1) The data in low temperature region exhibit an exponential behavior. When the phonon contribution is removed, this becomes more clear. (2) The specific heat anomaly at T_c is very sharp showing a jump of about 100 mJ/mol·K^2, this value is about 3–5 times higher than the bare value of band structure calculation. Therefore we can imagine that the electron–boson coupling is very strong in this system. In Fig. 21, we show the temperature dependence of the electronic specific heat and the theoretical fitting using an s-wave model. Now the normal state specific heat has been removed. One can see that the low temperature part exhibits a very flat feature indicating a full gap behavior. However, in the intermediate temperature, there is a hump which may be induced by a second band effect. Hardy *et al.* also did a measurement on the same system,

they found that a two model fitting[50] can give rise to a very good description of the data.

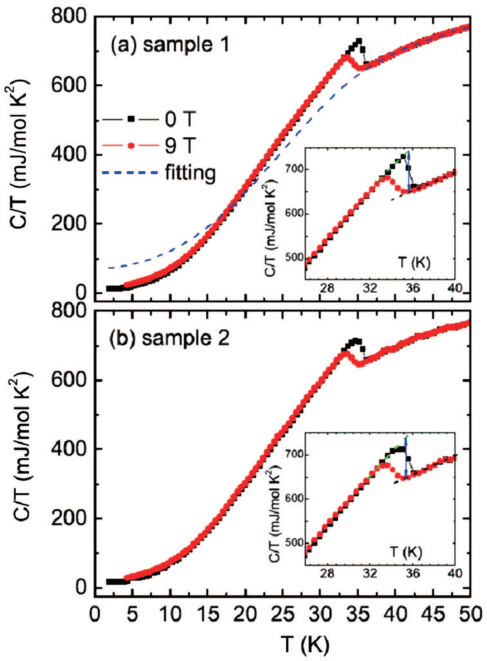


Fig. 20. (a) and (b) Raw data of temperature dependent specific heat coefficient C/T on two $Ba_{0.6}K_{0.4}Fe_2As_2$ samples at zero (dark square) and 9 T (red circle) magnetic fields. The insets show the specific heat anomaly near the transition point, showing a quite strong specific heat jump. The figure is copied from Ref. [51], APS Copyright.

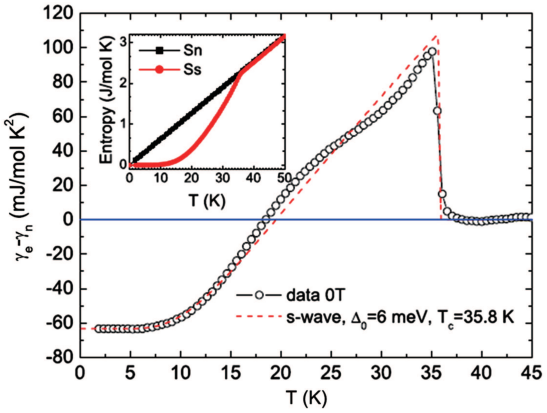


Fig. 21. The electronic specific heat after removing the phonon and the normal state electronic contributions in $Ba_{0.6}K_{0.4}Fe_2As_2$. The figure is copied from Ref. [51], APS Copyright.

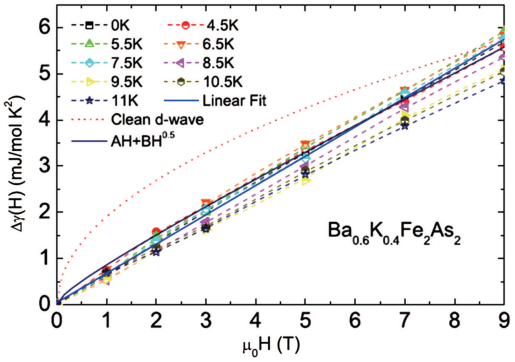


Fig. 22. Magnetic field dependence of specific heat of $Ba_{0.6}K_{0.4}Fe_2As_2$ in low temperature region. The figure is copied from Ref. [51], APS Copyright.

In order to check whether it is fully gapped, we present in Fig. 22 the magnetic field dependence of the electronic specific heat. One can see that in the zero temperature limit, the field induced specific heat shows a roughly linear field dependence, which strongly supports the fully gapped feature. Since $Ba_{0.6}K_{0.2}Fe_2As_2$ is a hole doped system, now the hole pocket takes the most weight of specific heat, therefore we can also conclude that the gap on the hole pocket shows a very good isotropic behavior in $Ba_{0.6}K_{0.4}Fe_2As_2$.

6.2. Specific heat investigation on $BaFe_{2-x}T_xAs_2$ (T = Co and Ni)

In the electron doped 122 system, the situation seems quite different from that in hole doped $Ba_{0.6}K_{0.4}Fe_2As_2$. First of all, a strong angle dependence has been found. In Fig. 23, we show the temperature dependence of the electronic specific heat in $BaFe_{2-x}T_xAs_2$ (T = Co and Ni). Now we use the very overdoped non-superconducting sample as the background to subtract the phonon contributions in the normal state. First of all, the isotropic s-wave fitting cannot work very well, with either single or double components. However, a combination of an s-wave and an extended s-wave can give a quite good fitting. To our surprise is that the single d-wave fitting can also give quite nice consistency with the data. This may suggest that a d-wave gap is also possible. However, the magnetic field dependence of specific heat shows a rough linear behavior again, which is against the d-wave fitting. Therefore we conclude that the gap may be highly anisotropy. But it remains unclear

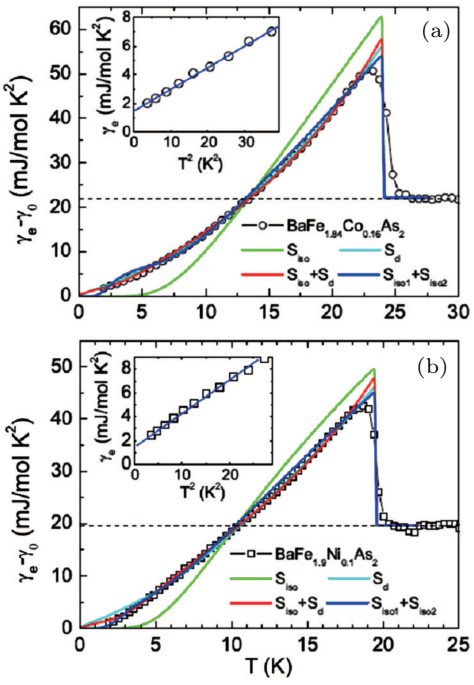


Fig. 23. Temperature dependence of electronic specific heat of optimally doped (a) $BaFe_{1.84}Co_{0.16}As_2$ and (b) $BaFe_{1.9}Ni_{0.1}As_2$. One can see that it is quite different from the case of $Ba_{0.6}K_{0.4}Fe_2As_2$. The low temperature data show some kind of positive curvature, but it is certainly not flattened as an s-wave. The figure is copied from Ref. [52], APS Copyright.

where the deep gap minimum locates. One possibility is that the gap minimum still locates at the hole pocket with a small segment of Fermi surface of gapless or gap minimum, due to the multi-orbital feature. The other possibility would be that the gap minimum locates at the electron Fermi pockets, since the samples now are electron doped and the electron pockets near the corner of the Brillion zone become quite large and the gap is highly anisotropic in these electron doped systems. In Fig. 24, we show the specific heat coefficient under magnetic field, one can see that they exhibit roughly a linear behavior. Combining this linear magnetic field dependence feature with the global fitting, we believe that the gap on the electron Fermi surface should be highly anisotropic.

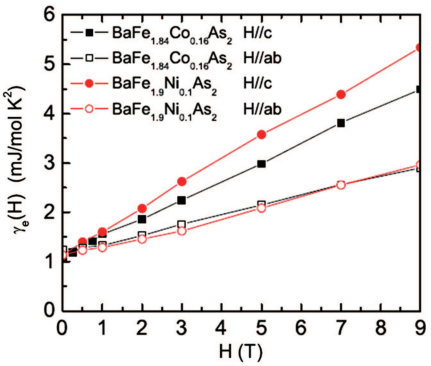


Fig. 24. Magnetic field dependence of enhancement of electronic specific heat in $BaFe_{1.84}Co_{0.16}As_2$ and $BaFe_{1.9}Ni_{0.1}As_2$. A rough linear behavior suggests fully gapped feature. The figure is copied from Ref. [52], APS Copyright.

6.3. Specific heat investigation on FeSe bulk sample

In order to study the superconducting gap structures of the FeSe bulk system, we have measured the specific heat of FeSe single crystals.[55] The temperature dependence of specific heat at zero field for one sample is presented in Fig. 25(a). One can see that the specific heat anomaly is quite clear with a value of about 10 mJ/mol·K^2. The normal state specific heat can be fitted with a polynomial function and thus it can be removed. The electronic contribution of specific heat is shown in Fig. 25(b), one can see that the specific heat jump is quite sharp without a very small tail in the normal state. This kind of tail has been observed in many cuprate superconductors which was interpreted as the strong superconducting fluctuation. Besides that, we see a small specific heat anomaly or jumping-up at about 1.08 K, which we argue that it might be the long sought antiferromagnetic order. In Fig. 26, we present the two-band model fitting to the data with many different models: (a) single s-wave gap, $\Delta(\theta)=\Delta_0$, (b) single d-wave $\Delta(\theta)=\Delta_0\cos 2\theta$, (c) single extended s-wave gap $\Delta(\theta)=\Delta_0(1+\alpha\cos 2\theta)$, (d) a combination of an s-wave and an extended s-wave. The best fitting as judged from both the fitting quality in wide temperature region and the entropy conservation of the low temperature anomaly is the two-band model fitting with a highly anisotropic gap $\Delta(\theta)=\Delta_0(1+\alpha\cos 2\theta)$ with $\alpha\approx 0.9$–1, see Figs. 23(b) and 23(c). This indicates that the gap minimum is quite small, in the scale of about 0.15–0.3 mV. This conclusion is quite consistent with the STM measurements.[56] The gaps on the hole derivative α-pocket and on the electron derivative ε-pocket both are highly anisotropic.

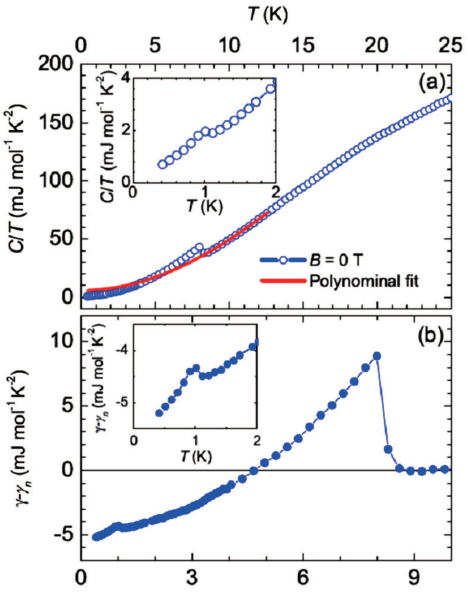


Fig. 25. (a) Specific heat of FeSe bulk sample. The red solid line represents the polynomial fit to the normal state. There is a small specific heat anomaly at about 1.08 K, which may be induced by the possible antiferromagnetic ordering. (b) The electronic specific heat after the normal state contribution is removed. The figure is copied from Ref. [55], APS Copyright.

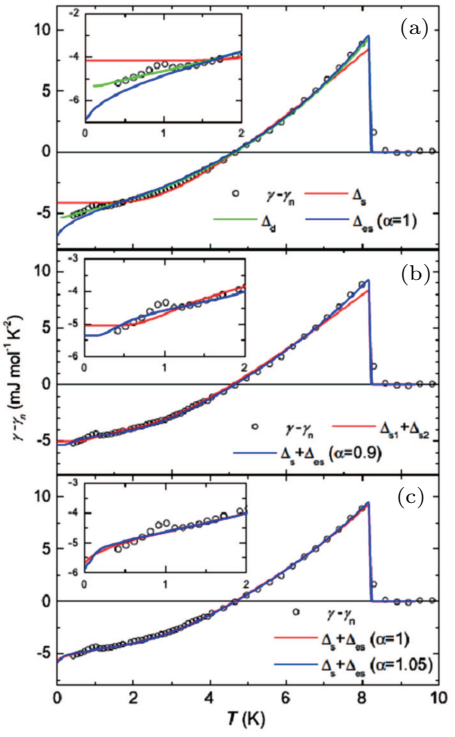


Fig. 26. Fitting to the electronic specific heat with many different models (see text). The best fitting, judged from both the fitting quality in wide temperature region and the entropy conservation of the low temperature anomaly, is the two-band model fitting with a highly anisotropic gap $\Delta(\theta)=\Delta_0(1+\alpha\cos 2\theta)$ with $\alpha\approx 0.9$–1, see panles (b) and (c). The figure is copied from Ref. [55], APS Copyright.

We also measured the magnetic field dependence of specific heat in FeSe bulk samples, the data are presented in Fig. 27. It is found that a magnetic field of about 14 T has already turned the sample completely into the normal state. However, as shown in Fig. 27(b), the magnetic field dependence of specific heat in the zero temperature limit can be fitted to a function $\Delta\gamma = pB + q\sqrt{B}$ with $(p : q \approx 2 : 5)$. This formula contains a linear part and a quadratic part, which is deviated from a linear behavior for an isotropic gap. However, it is also different from the Volovik relation, which clearly suggests that the d-wave pairing gap is not appropriate. A reasonable picture would be that the gap is highly anisotropic. This is consistent with the fitting to the temperature dependence of the electronic specific heat in Fig. 23 and is consistent with the STM data.[58] In iron based superconductors, the gap structure is mainly nodeless but highly anisotropic. This is in general consistent with the spin fluctuation mediated pairing manner, leading to the gap structure of $s^{\pm}$.[59,60]

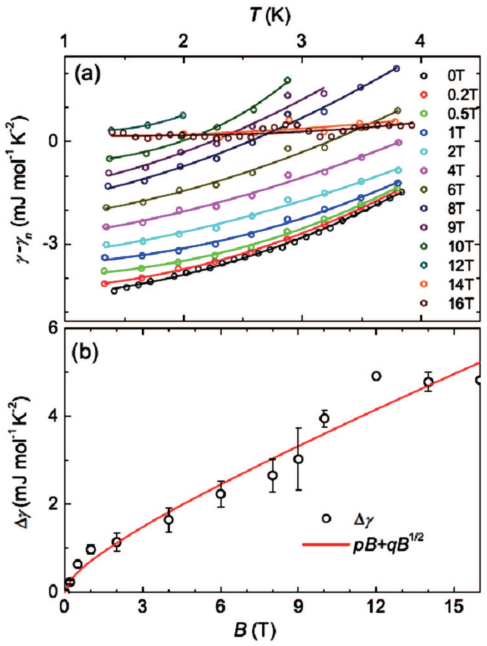


Fig. 27. Magnetic field induced change of specific heat coefficient. (a) The raw data (symbols) and the fitting curves for each magnetic field. The fitting range varies depending on the region of the specific heat anomaly which should not be involved in deriving the low temperature intercept. (b) The magnetic field induced specific heat coefficient $\Delta\gamma = [C(h) - C(0)]/T|_{T\to 0}$. The red solid line gives a combination of two terms, i.e., $\Delta\gamma = pB + q\sqrt{B}$ with $(p : q \approx 2 : 5)$.

7. Summary and concluding remarks

In this paper, we give a brief introduction to specific heat in superconductors. The core issue is the low energy quasiparticle excitations in the mixed state of type-II superconductors, which can be measured by low temperature specific heat. We first give an introduction to the fundamental physics concerning the quasiparticle excitations under the picture of different gap symmetries. Then we present the experimental data in cuprates and iron based superconductors. In cuprates, the low energy quasi-particle excitations show the feature of d-wave gap, but the problem is mainly about the pseudogap state which makes the Fermi surface truncated in the underdoped region, leading to the so-called Fermi arc/pocket as the ground state. Based on the this picture, we find that the superconducting condensation can be undertood as the "gap" on the Fermi arcs, namely, the energy scales on the terminals of the Fermi arcs determine the superconducting transition temperature. In the overdoped region of cuprate superconductors, when the Fermi surface becomes complete, a standard d-wave is recovered, although we have a lot of unpaired electrons. In iron based superconductors, we show data mainly in three systems, $Ba_{1-x}K_xFe_2As_2$, $BaFe_{2-x}T_xAs_2$ (T = Co or Ni), and FeSe bulk. The low temperature specific heat can be understood as nodeless gaps, but can be highly anisotropic, like in FeSe. This is consistent with the pairing gap structure of $s^{\pm}$.

Acknowledgement

This paper was written based on the past works in our group, thus we acknowledge all the contributors in these works.

References

[1] Clogston A M 1962 *Phys. Rev. Lett.* **9** 266
[2] Chandrasekhar B S 1962 *Appl. Phys. Lett.* **1** 7
[3] Tsuei C C and Kirtley J R 2000 *Rev. Mod. Phys.* **72** 969
[4] Timusk T and Statt B 1999 *Rep. Prog. Phys.* **62** 61
[5] Hussey N E 2002 *Adv. Phys.* **51** 1685
[6] Xiang T 2000 *d-wave superconductivity* (Beijing: Scientific Publishing Company)
[7] Wen H H, *et al*. 2005 *Phys. Rev. B* **72** 134507
[8] Wen H H, *et al*. 2004 *Phys. Rev. B* **70** 214505
[9] Caroli C and de Gennes P G 1964 *J. Matricon. Phys. Letts.* **9** 307
[10] Gygi F and Schluter M 1991 *Phys. Rev. B* **43** 7609
[11] Hayashi N and Ichioka M 1998 *K. Machida. Phys. Rev. Lett.* **80** 2921
[12] Hess H F, *et al*. 1990 *Phys. Rev. Lett.* **64** 2711
[13] Volovik G E 1993 *JETP Lett.* **58** 469
[14] Wen H H 2008 *J. Phys. Chem. Solids* **69** 3236
[15] Kopnin N B and Volovik G E 1996 *JETP Lett.* **64** 690
[16] Simon S H and Lee P A 1997 *Phys. Rev. Lett.* **78** 1548
[17] Volovik G E 1997 *JETP Lett.* **65** 491
[18] Kübert C and Hirschfeld P J 1998 *Solid State Commun.* **105** 459
[19] Wang Y, *et al*. 2007 *Phys. Rev. B* **76** 064512
[20] Moler K A, *et al*. 1997 *Phys. Rev. B* **55** 3954
[21] Garg A, *et al*. 2008 *Nat. Phys.* **4** 762
[22] Wen X G and Lee P A 1998 *Phys. Rev. Lett.* **80** 2193
[23] Norman M R, *et al*. 1998 *Nature* **392** 157
[24] Orenstein J and Millis A J 2000 *Science* **288** 480
[25] Norman M R, *et al*. 2005 *Adv. Phys.* **54** 715
[26] Damascelli A, *et al*. 2003 *Rev. Mod. Phys.* **75** 473
[27] Ding H, *et al*. 1996 *Nature* **382** 51
[28] Sutherland M, *et al*. 2003 *Phys. Rev. B* **67** 174520
[29] Alloul H, *et al*. 1991 *Phys. Rev. Lett.* **67** 3140
[30] Renner C, *et al*. 1998 *Phys. Rev. Lett.* **80** 149
[31] Loram J, *et al*. 1998 *Research Review, University Cambridge* (IRC in Superconductivity, London), p. 77
[32] Yoshida T, *et al*. 2006 *Phys. Rev. B* **74** 224510
[33] Junod A 1990 *Physical Properties of HTSC II* (Ginsberg D, Ed.) (Singapore: World Scientific)

[34] Phillips N E, *et al*. 1992 *Progress in Low Temperature Physics* (Brewer D F, Ed.) (Amsterdam: Elsevier Science Publishers B V)
[35] Fisher R A, *et al*. 2007 *Handbook of High-Temperature Superconductivity: Theory and Experiment* (Schrieffer J R and Brooks J S, Ed.) (Amsterdam: Springer-Verlag)
[36] Wright D A, *et al*. 1999 *Phys. Rev. Lett.* **82** 1550
[37] Chen S J, *et al*. 1998 *Phys. Rev. B* **58** R14753
[38] Fisher R A, *et al*. 2000 *Phys. Rev. B* **61** 1473
[39] Nohara M, *et al*. 2000 *J. Phys. Soc. Jpn.* **69** 1602
[40] Revaz B, *et al*. 1998 *Phys. Rev. Lett.* **80** 3364
[41] Wen H H and Wen X G 2007 *Physica C* **460–462** 28
[42] Badoux S, *et al*. 2016 *Nature* **531** 210
[43] Nakano T, *et al*. 1998 *J. Phys. Soc. Jpn.* **67** 2622
[44] Panagopoulos C and Xiang T 1998 *Phys. Rev. Lett.* **81** 2336
[45] Loram J W, *et al*. 2001 *J. Phys. Chem. Solids* **62** 59
[46] Matsuzaki T, *et al*. 2004 *J. Phys. Soc. Jpn.* **73** 2232
[47] Tallon J L, *et al*. 1995 *Phys. Rev. B* **51** R12911
[48] Li S L 2011 *Annu. Rev. Condens. Matter Phys.* **2** 121
[49] Chu C W 2009 *Nat. Phys.* **5** 787
[50] Hardy F, *et al*. 2010 *Europhys. Lett.* **91** 47008
[51] Mu G, *et al*. 2009 *Phys. Rev. B* **79** 174501
[52] Zeng B, *et al*. 2011 *Phys. Rev. B* **83** 144511
[53] Hardy F, *et al*. 2013 *Phys. Rev. Lett.* **111** 027002
[54] Xing J, *et al*. 2014 *Phys. Rev. B* **89** 140503
[55] Chen G Y, Zhu X Y, Yang H and Wen H H 2017 *Phys. Rev. B* **96** 064524
[56] Ding H, *et al*. 2008 *EPL* **83** 47001
[57] Shan L, *et al*. 2011 *Phys. Rev. B* **83** 060510
[58] Sprau P O, *et al*. 2017 *Science* **357** 75-80
[59] Mazin I I, *et al*. 2008 *Phys. Rev. Lett.* **101** 057003
[60] Kuroki K, *et al*. 2008 *Phys. Rev. Lett.* **101** 087004